



OPEN ACCESS

EDITED BY

Meng Zhang,
Northumbria University, United Kingdom

REVIEWED BY

Samantha Bryan,
University of Nottingham,
United Kingdom
Laura Zorzetto,
Max Planck Institute of Colloids and
Interfaces, Germany

*CORRESPONDENCE

Michael Gelinsky,
✉ michael.gelinsky@tu-dresden.de

SPECIALTY SECTION

This article was submitted to
Biomaterials,
a section of the journal
Frontiers in Bioengineering and
Biotechnology

RECEIVED 15 January 2023

ACCEPTED 20 March 2023

PUBLISHED 03 April 2023

CITATION

Reinhardt O, Ihmann S, Ahlhelm M and
Gelinsky M (2023), 3D bioprinting of
mineralizing cyanobacteria as novel
approach for the fabrication of living
building materials.

Front. Bioeng. Biotechnol. 11:1145177.
doi: 10.3389/fbioe.2023.1145177

COPYRIGHT

© 2023 Reinhardt, Ihmann, Ahlhelm and
Gelinsky. This is an open-access article
distributed under the terms of the
[Creative Commons Attribution License
\(CC BY\)](https://creativecommons.org/licenses/by/4.0/). The use, distribution or
reproduction in other forums is
permitted, provided the original author(s)
and the copyright owner(s) are credited
and that the original publication in this
journal is cited, in accordance with
accepted academic practice. No use,
distribution or reproduction is permitted
which does not comply with these terms.

3D bioprinting of mineralizing cyanobacteria as novel approach for the fabrication of living building materials

Olena Reinhardt¹, Stephanie Ihmann², Matthias Ahlhelm² and Michael Gelinsky^{1*}

¹Centre for Translational Bone, Joint and Soft Tissue Research, Faculty of Medicine Carl Gustav Carus, Technische Universität Dresden, Dresden, Germany, ²Biologized Materials and Structures, Fraunhofer Institute for Ceramic Technologies and Systems IKTS, Dresden, Germany

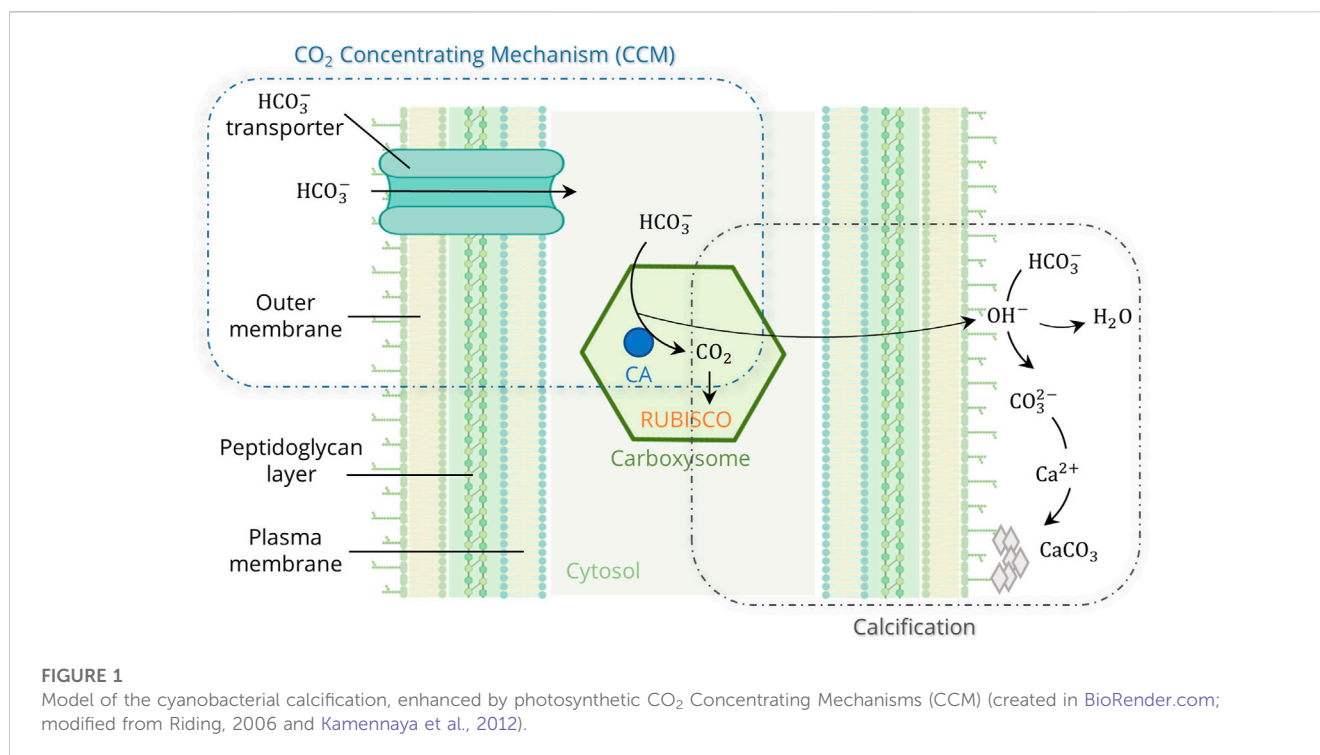
Living building materials (LBM) are gaining interest in the field of sustainable alternative construction materials to reduce the significant impact of the construction industry on global CO₂ emissions. This study investigated the process of three-dimensional bioprinting to create LBM incorporating the cyanobacterium *Synechococcus* sp. strain PCC 7002, which is capable of producing calcium carbonate (CaCO₃) as a biocement. Rheology and printability of biomaterial inks based on alginate-methylcellulose hydrogels containing up to 50 wt% sea sand were examined. PCC 7002 was incorporated into the bioinks and cell viability and growth was characterized by fluorescence microscopy and chlorophyll extraction after the printing process. Biomineralization was induced in liquid culture and in the bioprinted LBM and observed by scanning electron microscopy, energy-dispersive X-ray spectroscopy, and through mechanical characterization. Cell viability in the bioprinted scaffolds was confirmed over 14 days of cultivation, demonstrating that the cells were able to withstand shear stress and pressure during the extrusion process and remain viable in the immobilized state. CaCO₃ mineralization of PCC 7002 was observed in both liquid culture and bioprinted LBM. In comparison to cell-free scaffolds, LBM containing live cyanobacteria had a higher compressive strength. Therefore, bioprinted LBM containing photosynthetically active, mineralizing microorganisms could be proved to be beneficial for designing environmentally friendly construction materials.

KEYWORDS

biomineralization, three-dimensional printing, living building materials, engineered living materials, biocement, *Synechococcus* sp, MICP, microbially induced carbonate precipitation

1 Introduction

Using a variety of materials and a variety of structures and geometries created from 3D model data, the additive manufacturing (AM) process of three-dimensional (3D) printing opens up a vast range of potential applications (Murphy and Atala, 2014; Ngo et al., 2018; Praveena et al., 2022). The construction industry has recently developed interest in the AM technology (Khoshnevis, 2004; Wu et al., 2016; Kazemian et al., 2017). The benefits include freedom of design, individuality, and complexity of the structures (Labeaga-Martínez et al., 2017; Ngo et al., 2018). Concrete is the most common material utilized in building with AM



(Schutter et al., 2018). It is easy to process when it is fresh and reaches high compressive strength when cured (Guamán-Rivera et al., 2022). However, the building sector is responsible for 39% of global carbon dioxide (CO₂) emissions, with concrete alone accounting for 11% of global CO₂ emissions and thus significantly contributing to climate change (Concrete needs to lose its colossal carbon footprint, 2021; Architecture, 2022). Due to population growth and progressing urbanization, global demand for concrete will increase by up to 23% by 2050 (Architecture, 2022). To limit further global warming to +2°C by 2050, a significant reduction of CO₂ emissions by 24% is required. Therefore, new innovative technologies are needed that enable the reuse of existing materials (Tam, 2008; Noguchi et al., 2011), the reduction of total material demand (Khan et al., 2012; Panesar and Zhang, 2020; Zeybek et al., 2022), and the use of carbon-depleting materials (IEA, 2018; Concrete needs to lose its colossal carbon footprint, 2021).

A look at nature shows that worldwide there are natural producers of a biological cement consisting mainly of calcium carbonate (CaCO₃) (Strong and Eadie, 1978; Thompson et al., 1997; Foster et al., 2009). One of the oldest types of mineralizing microorganisms on Earth are cyanobacteria, which have been detected in about 2.8 billion years old fossil mats called stromatolites. Because they generate energy through oxygenic photosynthesis, enormous amounts of oxygen were produced as a waste product of their metabolism, allowing the first aerobic life forms to emerge. Cyanobacteria are thus considered to have paved the way for life (Tetsch, 2016). Even today, they are of great ecological importance, sequestering about 40% of annual CO₂ emissions from the atmosphere (Falkowski, 1994). Over 25% of global photosynthesis is carried out by only two genera, *Prochlorococcus* and *Synechococcus* (Whitman et al., 1998; Partensky et al., 1999). In addition to photosynthesis, the second

pathway in cyanobacteria for CO₂ fixation is Microbially Induced Carbonate Precipitation (MICP) (Golubic, 1973; Pentecost and Riding, 1986; Merz, 1992). This natural calcification occurs, for example, in stromatolites or whitening events, where cyanobacteria grow exponentially and mineralize dissolved inorganic carbon (HCO₃⁻ or CO₃²⁻) to calcium carbonate (CaCO₃) in the presence of high Ca²⁺ concentrations (Robbins and Blackwelder, 1992; Thompson et al., 1997; Foster et al., 2009). Cyanobacteria reduce the kinetic barriers and promote mineral formation through various metabolic reactions. They can cope with low CO₂ concentrations due to carbon concentrating mechanisms (CCM) that actively transport inorganic carbon compounds (HCO₃⁻) into the cell, where they accumulate in the carboxysomes and are converted to CO₂ by the enzyme Carbonic Anhydrase (CA) (Figure 1). CCM increase the local CO₂ concentration at the carboxylation site of the enzyme ribulose-1,5-bisphosphate carboxylase-oxygenase (RUBISCO) by up to a thousand-fold (Badger and Price, 2003; Price et al., 2008). During photosynthesis, RUBISCO utilizes CO₂ for energy generation (ATP). OH⁻ is released as a by-product during the conversion of HCO₃⁻ to CO₂, leading to an alkalization of the microenvironment. Additionally, Ca²⁺ accumulates at the cell surface, through transportation by Ca²⁺/H⁺ antiporters and chemical attraction to the negatively charged bacterial cell surface (Arp et al., 2001). These effects lead to supersaturation and the eventual formation of CaCO₃ on the outer cell surface (Thompson and Ferris, 1990; Merz, 1992).

In addition to cyanobacteria, there are other microorganisms capable of MICP, such as sulfate-reducing bacteria (Perito and Mastromei, 2011; Alshalif et al., 2016; Tambunan et al., 2019), microorganisms that utilize organic acids (Rodriguez-Navarro et al., 2003; Chekroun et al., 2004; Zhu and Dittrich, 2016), and microorganisms that are involved in a nitrogen cycle (Ersan et al.,

2015; Zhu and Dittrich, 2016). Dhimi et al. (2013b) describe the ureolytic pathway as the most easily controllable mechanism with the potential for rapid CaCO_3 production. The potential of ureolytic MICP has been analyzed in a variety of engineering applications, including sequestration of inorganic contaminants (Mitchell and Ferris, 2005), soil stabilization (DeJong et al., 2010), prevention of CO_2 leakage from geological reservoirs (Phillips et al., 2001), and crack repair in concrete (Wang et al., 2014; Belie et al., 2018). Recently, MICP of ureolytic bacteria in 3D printed and casted structures was shown to be potentially applied as artificial corals to help restoring marine reefs (Hirsch et al., 2023). However, the major disadvantage of the ureolytic MICP is the production of ammonia as a by-product, which has potentially toxic effects on living organisms and vegetation and could lead to eutrophication or acidification of ecosystems (Dhimi et al., 2013b). Another drawback is the production of endospores that can cause uncontrollable germination (Muynck et al., 2010).

Recently, photosynthetic MICP performed by cyanobacteria has received more attention in several engineering approaches because they serve as a carbon capture system by absorbing CO_2 during growth and mineralization (Heveran et al., 2020; Beatty et al., 2022; Sidhu et al., 2022). Heveran et al. (2020) investigated the inclusion of mineralizing cyanobacteria in a gelatin-hydroge-sand mixture by gel casting and demonstrated promising results in terms of the creation of consolidated constructs, probably caused by cyanobacteria-induced CaCO_3 mineralization, which improved the mechanical properties of such building materials. The application of MICP in the construction industry is becoming increasingly important. In the future, biomineralized cement could partly replace conventional cement in certain non-load-bearing applications to reduce overall CO_2 emissions of building materials. Following the example of rammed earth, an ancient construction technique, where 10–15 cm of soil is deposited and rammed in layers (Nouri et al., 2021), MICP-based building materials could be created through a layer-by-layer mineralization process.

In this study, the concept of cyanobacterial MICP was combined with the manufacturing method of 3D bioprinting, to investigate the possibility of producing biological cement (CaCO_3) in 3D printed constructs. Extrusion bioprinting with bioinks, hydrogels containing living cells, is an established technique especially in the biomedical and tissue engineering field (Malda et al., 2013; Kilian et al., 2017; Valot et al., 2019; Ahlfeld et al., 2020), but there are also increasing applications in biotechnology (Krujatz et al., 2022). Bioprinting like every AM technology allows the manufacturing of 3D constructs of predefined outer and inner morphology based on computer-aided design. In case of bioprinted tissue samples, the presence of suitable open porosity has been demonstrated to be beneficial for cell survival and development, especially in case of volumetric objects (Khalighi and Saadatmand, 2021). In this study, a bioink consisting of alginate, methylcellulose, and sea sand was used to incorporate the cyanobacterium *Synechococcus* sp. strain PCC 7002. *Synechococcus* species are ubiquitous in marine and freshwater environments, their calcification ability is well understood and has been analyzed in several studies, and they are known to be stable towards environmental stress (e.g., high irradiation: up to $4.5 \text{ mE m}^{-2} \text{ s}^{-1}$ (Nomura et al., 2006), temperature: up to 42°C (Ludwig and Bryant, 2012), moisture (Heveran et al., 2020), and salinity changes: 3–300 mM NaCl (Ludwig and Bryant, 2012)). After the viability of the cells in the printed scaffolds was confirmed, the MICP of PCC 7002 was investigated

in liquid culture and in the bioprinted structures. The calcified structures are referred to as Living Building Materials (LBM), consisting of structural materials which create the backbone and living microorganisms that transform the structural properties and add biological function (Heveran et al., 2020).

2 Materials and methods

2.1 Bacterial strain and cultivation conditions

The cyanobacterium *Synechococcus* sp. strain PCC 7002 (further referred to as PCC 7002) was purchased from the Pasteur Collection of Cyanobacteria (Institut Pasteur, Paris, France). Cell growth was maintained in A+ medium containing 0.308 M NaCl, 0.02 M MgSO_4 , 0.08 mM Na_2EDTA , 8.05 mM KCl, 2.52 mM CaCl_2 , 11.8 mM NaNO_3 , 0.37 mM KH_2PO_4 , 8.26 mM Trizma Base (pH 8.2) and 10 mL/L Trace Components, consisting of 55.5 mM H_3BO_3 , 0.23 mM ZnCl_2 , 0.021 mM MoO_3 , 0.3 μM vitamin B_{12} , 0.14 mM FeCl_3 , 0.22 mM MnCl_2 , 0.12 μM CuSO_4 , 0.5 μM CoCl_2 (Stevens et al., 1973; Heveran et al., 2020). PCC 7002 was maintained in Erlenmeyer flasks in the light incubator Infors Multitron (Infors, Bottmingen, Switzerland) at 200 rpm, 24°C , and an illumination of $180 \mu\text{mol m}^{-2} \text{ s}^{-1}$ by cool white fluorescent lamps (Heveran et al., 2020).

2.2 Preparation and rheological characterization of the biomaterial inks

A hydrogel bioink based on alginate and methylcellulose (algMC) was prepared for extrusion-based bioprinting (Schütz et al., 2017; Ahlfeld et al., 2020). Alginic acid sodium salt (3 wt%; Sigma Aldrich, Taufkirchen, Germany) was dissolved into deionized water and sterilized by autoclaving at 120°C for 20 min. Methylcellulose powder (9 wt%; Sigma Aldrich) and sea sand (30/50 wt%; sieved to particle size $<0.25 \text{ mm}$; Carl Roth, Karlsruhe, Germany) were separately autoclaved at 120°C for 20 min, before being manually stirred into the alginate solution with a spatula. The homogeneous paste was incubated for 2 h to allow the methylcellulose to swell. Hereafter, the hydrogel will be referred to as algMC + x wt% sand. After swelling, 100 μL per g hydrogel of either a bacterial suspension (7×10^7 cells per gram bioink) or deionized water was added to the composite ink and mixed homogeneously.

Rheological properties were analyzed using a rotary rheometer (Rheotest RN 4.1, Medingen, Germany) with a plate-plate measurement setup and a plate distance of 0.5 mm. Viscosity and shear-thinning properties were determined by applying a constantly increasing shear rate from 0 to 100 s^{-1} for 300 s ($n = 3$). Shear recovery was characterized by applying a constant shear rate of 5 s^{-1} for 200 s, followed by a shear rate of 500 s^{-1} for 100 s. This procedure was repeated twice ($n = 3$).

2.3 Printability characterization by filament fusion and filament collapse test

Printability was characterized by the filament fusion and filament collapse test, described by Ribeiro et al. (2017). Briefly,

the filament fusion test was performed by printing three layers of a meandering pattern with increasing strand spacing using the three-axial BioScaffolder plotter (BioScaffolder 3.1, GeSiM, Radeberg, Germany). The hydrogel was extruded through a nozzle with an inner diameter of 840 μm (Globaco, Rödermark, Germany). After plotting, the structures were imaged with a stereo light microscope (Leica M205 C with DFC295 camera, Wetzlar, Germany) and analyzed with the image software Fiji (ImageJ 1.53f51, Schindelin et al., 2012). Filament segment length and filament thickness were measured and the quotient of these measurements was evaluated as a function of the corresponding filament spacing. The measurements were performed with a sample size of $n = 5$.

The filament collapse test was performed by printing a single filament on a platform with pillars with the bioprinter BioScaffolder 3.1, with the gap distance increasing with every pillar (1, 2, 4, 8, 16 mm). Immediately after printing, a photo was taken and analyzed with the software Fiji. For the analysis, the angle of filament deflection was measured and plotted against the corresponding gap distance. The measurements were performed in triplicates.

2.4 Viability assessment and quantification of embedded cyanobacteria in the printed hydrogel scaffolds

The viability of PCC 7002 in bioprinted scaffolds was analyzed by fluorescence microscopy using the Keyence BZ-X700 (Keyence, Osaka, Japan). Living cells were determined by imaging the autofluorescence of chlorophyll (red). Dead cells were stained using the nucleic acid dye SYTOX Green (Invitrogen, Thermo Fisher Scientific, USA) (Sato et al., 2004; Schulze et al., 2011). First, scaffolds (10 mm \times 10 mm, $h = 3$ mm) were printed with an air pressure of 200 kPa and a plotting speed of 8 mm/s, a layer-to-layer orientation of 90 $^\circ\text{C}$ and a layer thickness of 0.56 mm with a 840 μm needle and a strand distance of 1.45 mm. These were ionically crosslinked with 100 mM CaCl_2 solution for 10 min and further cultured in 12-well plates (Corning, New York, USA) with 2 mL medium per well and scaffold. After certain cultivation time points, each scaffold was incubated in 2 mL deionized water containing 5 mM SYTOX Green for 15 min in the dark. Viability as a quotient of living cells to the sum of imaged cells was calculated using the image software Fiji.

To analyze the growth of the cyanobacteria in the bioprinted scaffolds, the chlorophyll content was determined. Bioprinted scaffolds were collected after 1, 3, 7, 10, and 14 days of cultivation and stored at -80 $^\circ\text{C}$ until further analysis. After thawing, 3 mL of 100 mM sodium citrate solution was added per scaffold to dissolve the constructs overnight at 4 $^\circ\text{C}$. After centrifugation of the dissolved samples at 12,000 rpm for 15 min, the supernatant was removed. The cyanobacterial pellet was resuspended in 250 μL dimethyl sulfoxide (DMSO, Sigma) and transferred to a Precellys tube (Peqlab, Erlangen, Germany), which was frozen at -80 $^\circ\text{C}$ for 20 min. After thawing, three ceramic Precellys beads (Peqlab) and 1 mL DMSO were added to the tube. The tube was transferred to the cell homogenizer (Precellys 24 system, Peqlab), where it was shaken three times for 30 s at 5,000 rpm. Into a transparent 96-well plate, 200 μL of

the lysate was added per well and the optical density was measured at 435 nm with a microplate reader (Infinite M200 pro, Tecan, Switzerland). Measurements were performed in triplicates.

2.5 Analysis of biomineralization

2.5.1 Biomineralization assay

The mineralization medium was prepared as described by Heveran et al. (2020). Briefly, an A+ medium without NaCl was prepared, and 100 mM NaHCO_3 was added, followed by adjusting the pH to 7.6, after which 100 mM of CaCl_2 was slowly added to the medium, which was finally sterile-filtered through a 0.2 μm cellulose acetate filter (Corning, New York, USA). Liquid culture biomineralization was performed by incubating 10 vol% of the preculture into the mineralization medium so that the initial optical density (OD) at 750 nm was 0.3. The suspension was cultured in the light incubator Infors Multitron for 24 h at 24 $^\circ\text{C}$, 200 rpm, and 180 $\mu\text{mol m}^{-2} \text{s}^{-1}$ illumination. For the biomineralization experiments with immobilized PCC 7002 2 mL of mineralization medium was added to each 3D-printed scaffold. The scaffolds (10 mm \times 10 mm, $h = 10$ mm) were printed with an air pressure of 200 kPa and a plotting speed of 8 mm/s, a layer-to-layer orientation of 90 $^\circ\text{C}$ and a layer thickness of 0.56 mm with a 840 μm needle and a strand distance of 1.45 mm. After ionic crosslinking with 100 mM CaCl_2 solution for 10 min, the scaffolds were cultured in the light incubator Infors Multitron at 24 $^\circ\text{C}$, 200 rpm, and 180 $\mu\text{mol m}^{-2} \text{s}^{-1}$ and removed from the medium for further analysis after 24 h, 7 days, and 14 days of cultivation.

2.5.2 Scanning electron microscopy (SEM) and energy dispersive X-ray (EDX) analysis

SEM images were acquired using the Philips XL 30/ESEM (operated in SEM mode), at a voltage of 3 kV (spot size 3). Before imaging, liquid samples were dropped onto a 0.2 μm cellulose acetate filter and washed twice with deionized water. After fixation with 3.7% formaldehyde for 30 min, samples were dehydrated with increasing ethanol concentrations, air-dried under a fume hood, and sputter-coated with gold. 3D-printed scaffolds were directly air-dried and sputter-coated with gold. EDX measurements were conducted with samples prepared as described for SEM above.

2.5.3 Mechanical properties

A uniaxial compressive test was performed to analyze the mechanical properties of fresh and dried 3D printed scaffolds after mineralization using a universal testing machine (Z010 with a 100 N and 10 kN load cell; Zwick, Germany). The scaffolds were fabricated as described above in 2.5.1. Fresh scaffolds were tested directly after removal from the mineralization medium, dried scaffolds were air-dried for 14 days at room temperature until weight equilibrium prior to the measurements. The uniaxial compressive test was performed with a speed of 0.2% l_0 per min and the compressive strength was analyzed.

2.6 Statistical analysis

Statistical analysis was performed using the software GraphPad Prism (GraphPad Software, Boston, USA). Grouped data were

analyzed by using one-way Analysis of Variance (ANOVA) and Tukey's method for multiple comparisons. In the graphical and numerical results, data are presented as mean \pm standard deviation. When differences between data points were $p < 0.05$, they were considered statistically significant.

3 Results

3.1 Characterization of bioinks with incorporated sea sand particles

To evaluate the suitability of extrusion-based bioprinting as a manufacturing method for LBM, an ink consisting of 3 wt% alginate and 9 wt% methylcellulose (algMC) was chosen, as it is known for its good printability, biocompatibility, and is well-established in the field of bioprinting of both mammalian and non-mammalian cells (Kilian et al., 2017; Seidel et al., 2017; Ahlfeld et al., 2020). The goal was to modify the ink with a support material that would later increase the stability of the LBM and serve as nucleation sites for CaCO_3 biomineralization. Sand was chosen as the support material because it is commonly used as fine aggregates in conventional concrete (Bos et al., 2016; Deutsches Institut für Normung, 2021).

The highest sand concentration tested in the algMC ink was 70 wt%. However, these composite hydrogels were very stiff and brittle, and therefore, not suitable for extrusion-based bioprinting. A homogenous paste was achieved with up to 50 wt% sand. To evaluate the suitability of the pastes for extrusion-based

bioprinting, the viscosity and shear recovery were analyzed (Figure 2). The incorporation of sand did not affect the shear-thinning behavior of the paste, which is an essential property for printability in extrusion-based processes. At a low shear rate of 5 s^{-1} , the viscosity increased with higher sand concentrations, from $390 \pm 80 \text{ Pa s}$ in algMC to $493 \pm 125 \text{ Pa s}$ with 30 wt% sand, and to $642 \pm 94 \text{ Pa s}$ with 50 wt% sand. At a high shear rate of 100 s^{-1} , the viscosity with and without sand was approximately the same at $21 \pm 8 \text{ Pa s}$, $21 \pm 7 \text{ Pa s}$, and $22 \pm 14 \text{ Pa s}$, respectively.

Furthermore, the shear recovery was analyzed to investigate the recovery potential of the algMC biomaterial inks with increasing sand concentration (Kesti et al., 2016; Paxton et al., 2017). A low (5 s^{-1}) and high shear rate (100 s^{-1}) were alternately applied, and viscosity was measured. Figure 2B shows that recovery in viscosity was observed for all hydrogels. However, after the first loading at high shear rates, the viscosity did not recover completely to the initial state at low shear rates. After further loading at high shear rates, it recovered to the state after the first high shear loading. This indicates the initial irreversible alteration of the polymeric structures (Ahlfeld et al., 2018).

To evaluate the shape fidelity of printed filaments, Ribeiro et al. proposed a filament collapse and filament fusion test (Ribeiro et al., 2017). Briefly, in the filament collapse test, a strand was printed on a bridge structure with increasing distance between the gaps (Figure 3A). The angle of the collapsing strand was measured using image analysis and plotted against the corresponding gap distance. The bending angle of the filament decreases with increasing sand content. At the maximum tested gap distance of

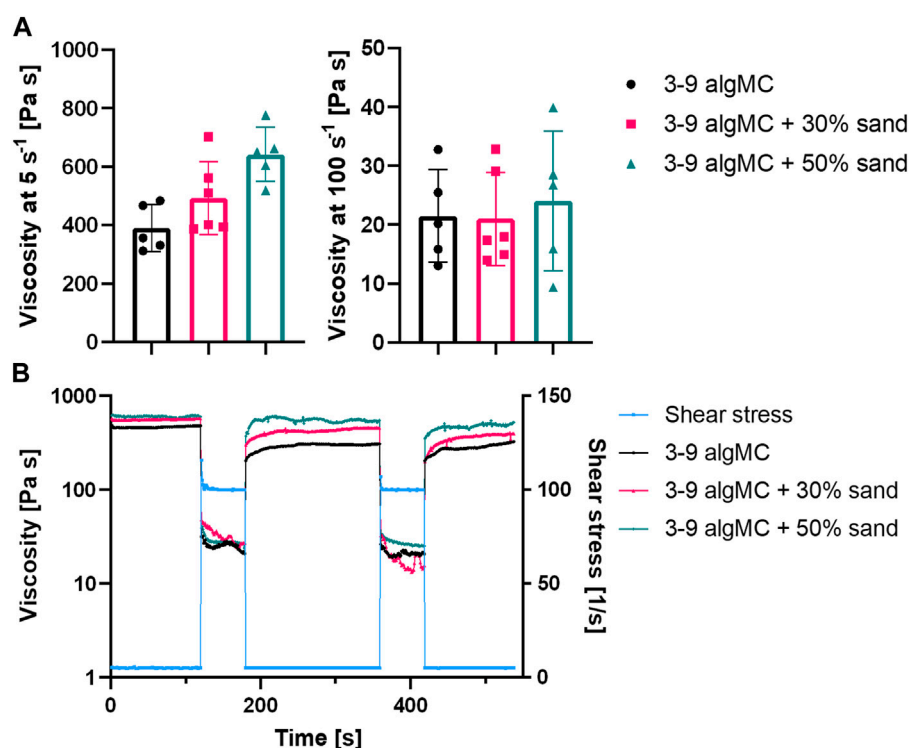


FIGURE 2

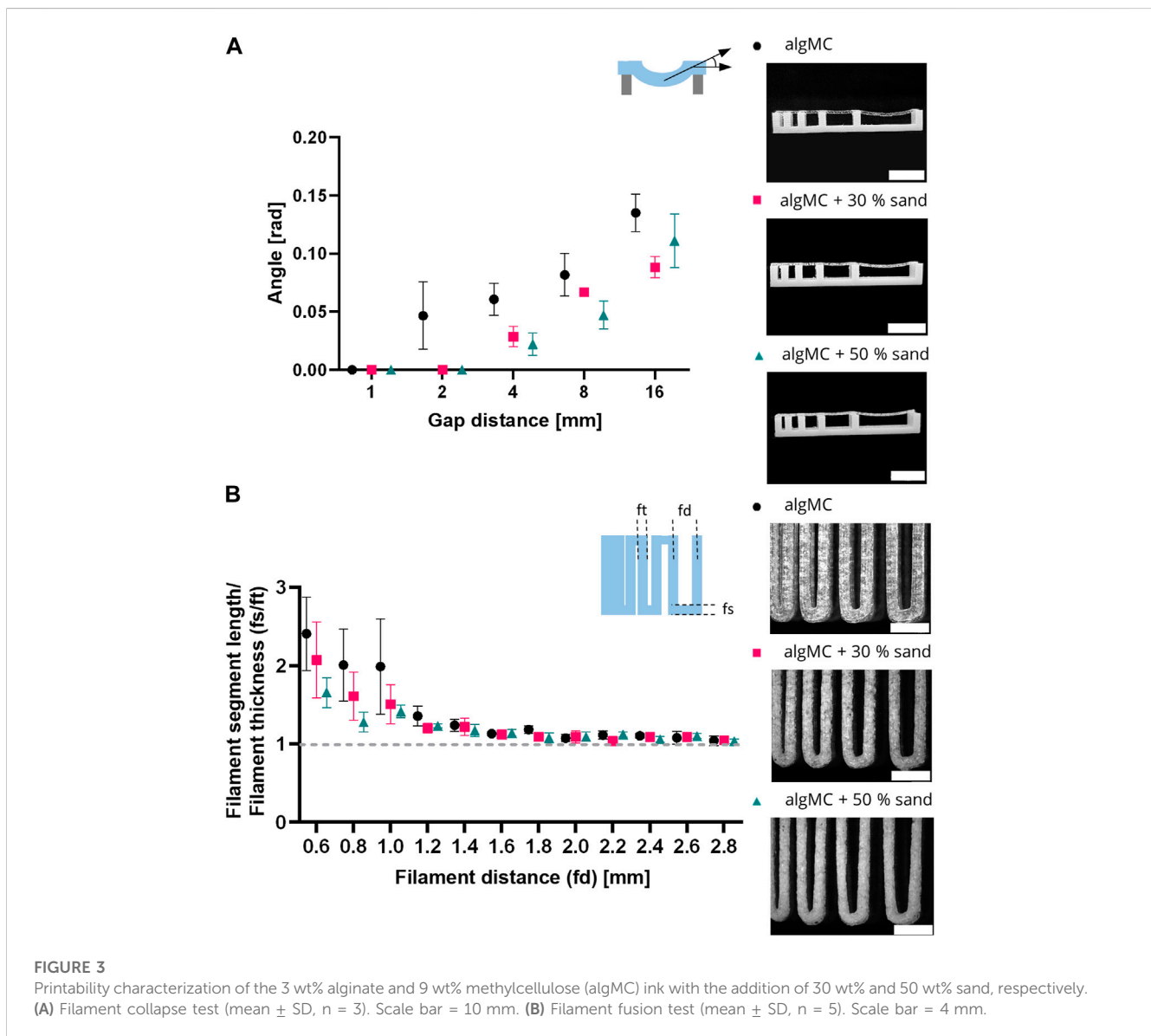
Rheological characterization of the 3 wt% alginate and 9 wt% methylcellulose (algMC) ink with the addition of 30 wt% and 50 wt% sand. (A) Viscosity of inks at low (5 s^{-1}) and high (100 s^{-1}) shear rates (mean \pm SD, $n \geq 5$); (B) Representative measurements of the shear recovery behavior.

16 mm, the angle decreases from 0.135 ± 0.016 rad in algMC to 0.088 ± 0.016 rad with 30 wt% sand to 0.111 ± 0.023 rad with 50 wt% sand. The higher viscosity at low shear rates, as shown above in Figure 2A, makes the material stiffer after printing with increasing sand concentrations.

In the filament fusion test, three strands were printed on top of each other in a meandering pattern with increasing strand distances. For analysis, filament segment length and filament thickness were measured, and their ratio was plotted against the corresponding filament distance (Figure 3B). For all inks tested the ratio of the segment length to the thickness decreased with increasing strand distance. Above a filament distance of 2 mm, the ratio of filament segment length to filament thickness was about 1 for all inks tested, which is desirable. In general, the ratios are smaller for the inks with sand particles than for the algMC ink, indicating better shape fidelity.

3.2 Viability of bioprinted PCC 7002

Since all ink formulations showed good printability and shape fidelity, *Synechococcus* sp. strain PCC 7002 (further referred to as PCC 7002) was added at a cell density of 7×10^7 cells per gram bioink to analyze the effect of the hydrogel and sand particles on the cell viability during a 14-day cultivation period. The viability in the bioprinted constructs was determined by image analysis of live/dead stained fluorescence images taken after 1, 3, 7, 10, and 14 days of cultivation (Figure 4A). Additionally, stereomicroscopic images (Figure 4C) and the chlorophyll content (Figure 4D) of the scaffolds on each time point were analyzed. Overall, the viability was very high for all tested bioinks, being $88.7 \pm 2.2\%$ (algMC), $86.2 \pm 4.9\%$ (algMC +30 wt% sand), and $79.9 \pm 8.7\%$ (algMC +50 wt% sand). No significant difference in cell viability between the three bioinks



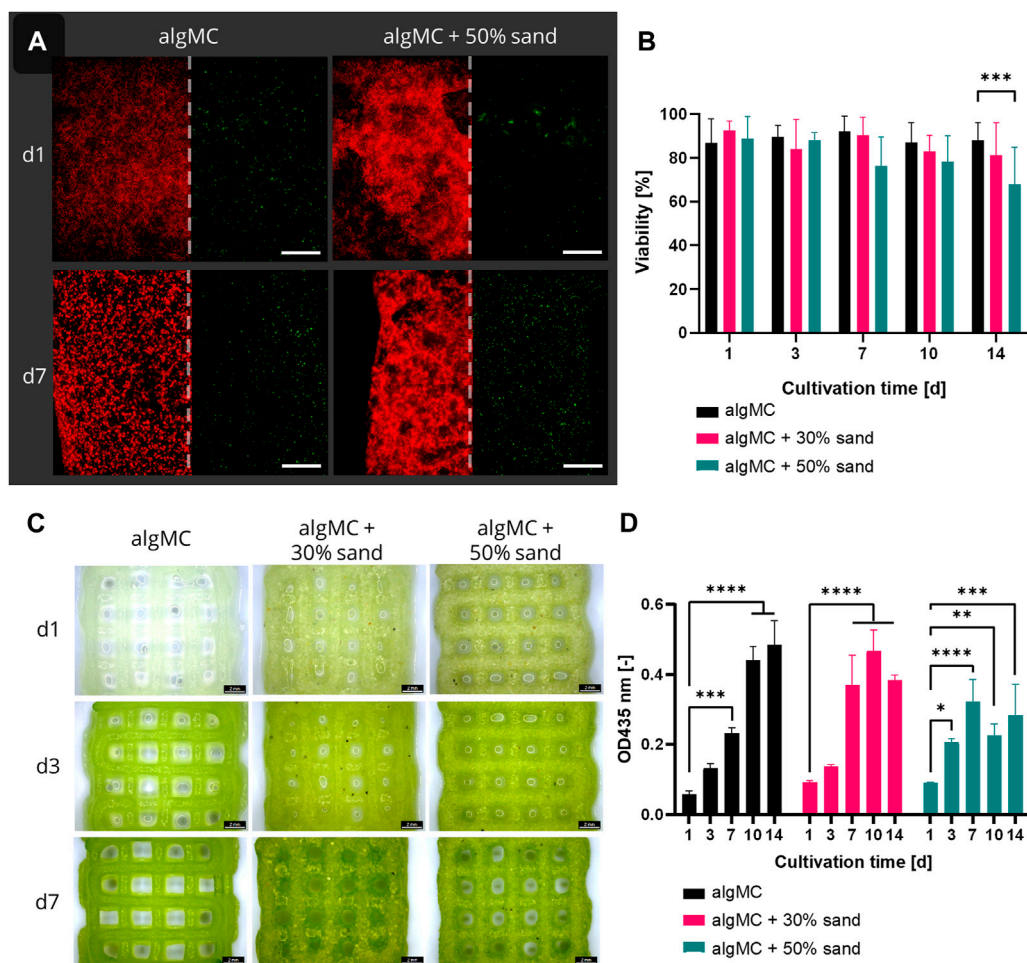


FIGURE 4

(A) Fluorescence microscope images of immobilized PCC 7002 in the algMC bioink with and without the addition of 50 wt% sand. Living cells show red autofluorescence (left), dead cells appear green (right). Scale bars = 200 μm . (B) Viability of PCC 7002 in the algMC bioink without, with 30 wt% and 50 wt% of sand, respectively, over a cultivation period of 14 days (data shows mean \pm SD, $n \geq 5$ of two individual experiments, $***p < 0.001$). (C) Stereoscopic images of algMC scaffolds without with 30, and with 50 wt% sand after 1, 3, and 7 days of cultivation. Scale bar = 2 mm. (D) Measurement of the optical density (OD) at 435 nm (chlorophyll content) over a cultivation period of 14 days (data shows mean \pm SD, $n = 3$, $*p < 0.05$, $**p < 0.01$, $***p < 0.001$, $****p < 0.0001$).

could be detected until day 10 (Figure 4B). Only on day 14 the viability of PCC 7002 in the ink with 50 wt% sand ($68.0 \pm 16.7\%$) was significantly lower than in the ink without sand ($88.0 \pm 8.2\%$). As on day 1 the viability was high in all tested bioinks (86.8–92.6%), the incorporated sand particles did obviously not damage the cyanobacteria through increased shear stress during the printing process. The chlorophyll content (optical density (OD) at 435 nm) increased significantly for all tested bioinks within the first 7 days of cultivation (Figure 4D). By this time, the OD at 435 nm increased 4.1 ± 0.2 -fold, 4.1 ± 0.8 -fold, and 3.6 ± 0.6 -fold compared to day 1 of cultivation in the algMC, algMC +30% sand, and algMC +50% sand bioinks, respectively. However, after 10 days of cultivation, cell outgrowth into the medium was observed in the samples with sand. This effect was stronger with increasing sand concentration and led to decreased chlorophyll measurements inside the scaffolds. After 14 days of cultivation, the OD at 435 nm was 0.48 ± 0.06 , 0.38 ± 0.01 , and

0.28 ± 0.07 in the algMC, algMC +30% sand, and algMC +50% sand bioinks, respectively.

3.3 Biomineralization in liquid culture and in bioprinted constructs

To ensure the calcifying ability of PCC 7002, a mineralization assay was first performed in liquid culture. Bacteria were cultured for 24 h in mineralization medium, containing 100 mM CaCl_2 and 100 mM NaHCO_3 . The samples were then analyzed by SEM (Figure 5) and EDX (not shown). Calcium-containing minerals were observed adjacent to or incorporating the bacterial cells, indicating microbial calcification. CaCO_3 was present in three different polymorphs—calcite, vaterite, and aragonite—that clearly can be distinguished by their morphological appearance by SEM as shown in Figure 5.

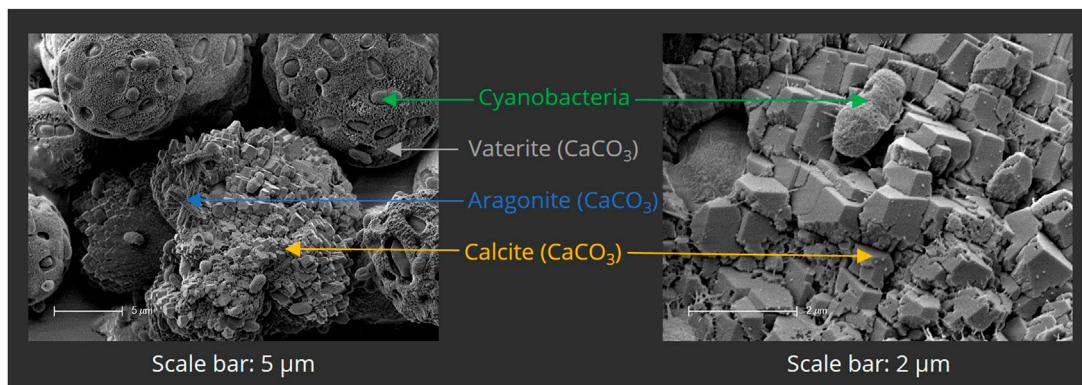


FIGURE 5 Scanning electron micrographs of mineralized PCC 7002 after 7 days of mineralization. Bacterial cells are surrounded by mineralized calcium carbonate (CaCO₃), present in the different polymorphs vaterite, aragonite and calcite.

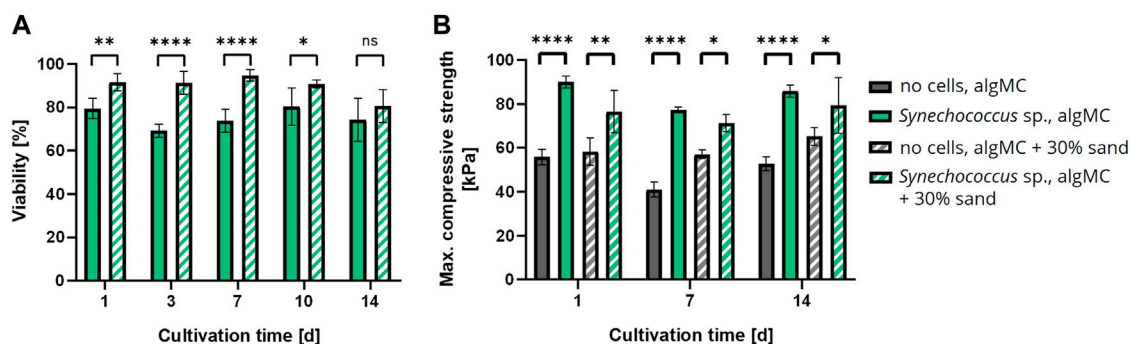


FIGURE 6 (A) Viability of bioprinted PCC 7002 in the algMC bioink without and with 30 wt% of sand over a cultivation period of 14 days (mean ± SD, n = 6, ****p < 0.0001, **p < 0.01, *p < 0.1). (B) Maximum compressive strength of wet scaffolds without cells (=abiotic control) and with PCC 7002 (=LBM) cultivated in mineralization medium for 1, 7, and 14 days (mean ± SD, n = 3, ****p < 0.0001, **p < 0.01, *p < 0.1).

Since biomineralization was observed in liquid culture, the next step was to induce biomineralization of the immobilized cells in the bioprinted constructs to create the LBM. Briefly, PCC 7002 was incorporated into the algMC bioink without and with 30 wt% of sand, at a cell density of 7×10^7 cells per gram bioink. After printing, the scaffolds were crosslinked for 10 min with 100 mM CaCl₂ and cultured in mineralization medium at 24 °C for up to 14 days. Cell viability was analyzed by fluorescence microscopy with image analysis and showed high viability in the LBM without and with 30 wt% of sand even after 14 days of cultivation in the mineralization medium, with a viability of $74.2 \pm 9.8\%$ and $80.6 \pm 7.6\%$ (n = 6), respectively (Figure 6A). A significantly higher viability in the scaffolds with 30 wt% sand was observed until day 10. However, after 14 days of cultivation, no significant difference regarding cell viability was measured between these bioinks.

In addition, the LBM and abiotic control (reference samples without cells) were mechanically analyzed by a uniaxial compression

test. The samples were removed from the mineralization medium after 1, 7, and 14 days and analyzed in wet conditions. The maximum compressive strength of all tested samples did not change significantly over time. However, all LBM with PCC 7002 showed significantly higher maximum compressive strength than the abiotic control at all time points (Figure 6B). After 1 day of mineralization, the maximum compressive strength of the LBM was about 38% and about 24% higher than in the abiotic control without and with 30 wt% of sand, respectively.

In addition to the analysis of the LBM in wet condition, air-dried LBM and abiotic control samples were also examined for their mechanical properties. For this assay, samples were printed with 30 and 50 wt% of sand, respectively, with and without cells, cultured in mineralization medium for 7 days and air-dried until weight equilibrium (Figure 7B). A uniaxial compression test was performed with the dry LBM and the abiotic control (Figure 7A). When comparing the stress at 50% strain, the lowest values were measured for the abiotic control with 50 wt% sand ($7.6 \pm$

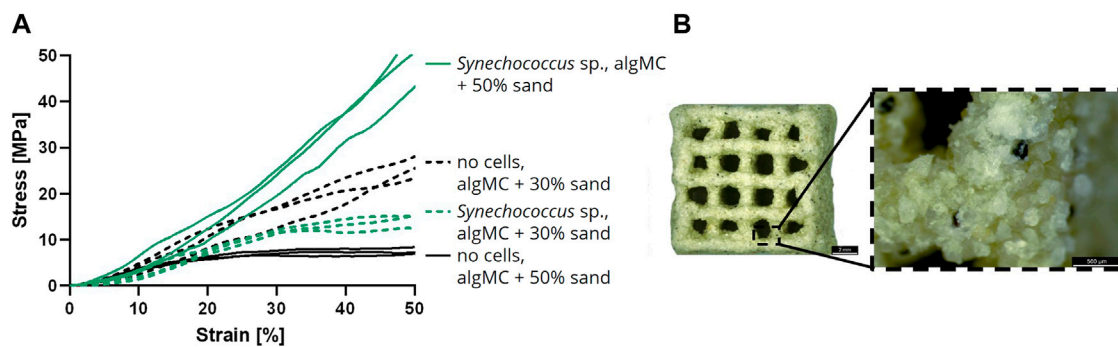


FIGURE 7

(A) Compressive stress over increasing strain of air-dried samples after the cultivation for 7 days in mineralization medium ($n = 3$). (B) Light microscope image of a dry mineralized sample with PCC 7002 and 50 wt% of sand. Scale bars represent 2 mm (left) and 500 μm (right).

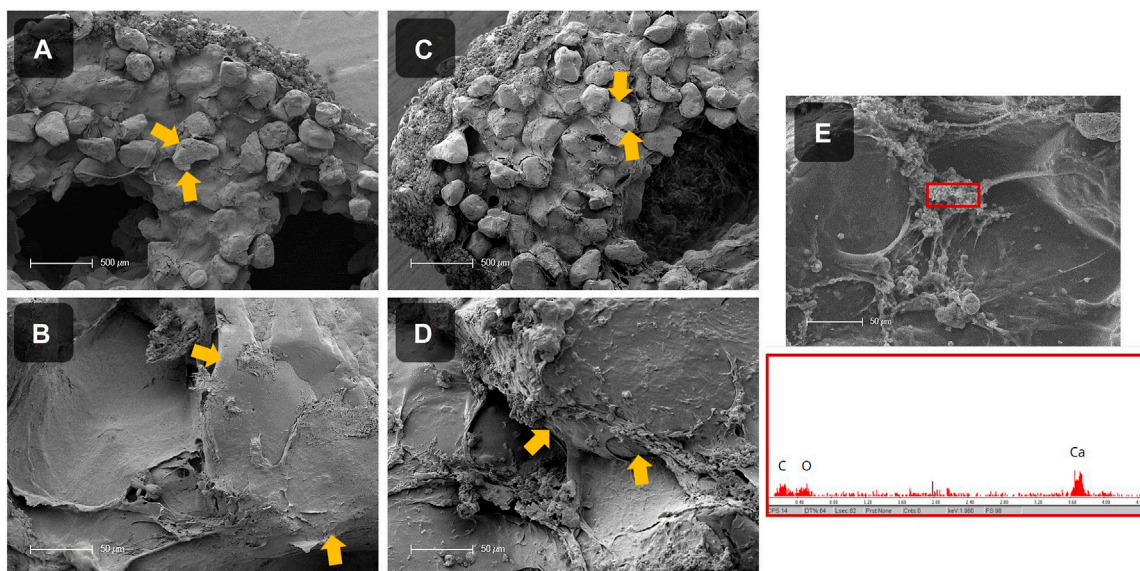


FIGURE 8

SEM images of the cross section of dried, mineralized scaffolds without cells (= abiotic control; (A, B)) and with PCC 7002 (= LBM; (C–E)) with 50 wt% of sand. Sand particles are marked with yellow arrows. EDX measurement of precipitates inside of the scaffold with PCC 7002, showing a calcium peak (E). Scale bars (A, C) = 500 μm , scale bars (B, D, E) = 50 μm .

0.8 MPa). The abiotic control with 30 wt% sand resulted in higher compressive strengths (25.7 ± 2.4 MPa). The LBM with PCC 7002 with 30 wt% sand had lower compressive strengths than the abiotic control (14.4 ± 1.5 MPa), but the LBM with 50 wt% sand yielded the highest compressive strengths measured (50.1 ± 6.3 MPa), 6.6 times higher than the respective control without cyanobacteria.

Besides the mechanical analysis, the mineralization inside the LBM was investigated by SEM and EDX measurements (Figure 8). Therefore, cross sections of LBM and abiotic control samples with 50 wt% sand were prepared, air-dried, sputtered with gold, and further analyzed. It was noticeable that the surfaces of both samples were covered with minerals. Inside the abiotic control, the alginates

matrix connecting the sand particles looked smooth and almost no mineral precipitates were detected (Figures 8A, B). In contrast, many minerals were visible in the LBM (Figures 8C, D). Analysis of the mineral phases by EDX revealed the presence of a calcium peak (Figure 8E), indicating the formation of calcium carbonate.

4 Discussion

Cyanobacteria have not only contributed greatly to the emergence of aerobic life forms in the past but are still of great importance today, especially for the capture and storage of CO_2 from the atmosphere (Falkowski, 1994; Whitman et al., 1998;

Tetsch, 2016). Their ability to mineralize CaCO_3 and simultaneously sequester CO_2 is a promising functionality that has been exploited within the concept of Living Building Materials (LBM) in this study to create environmentally friendly building materials. 3D bioprinting was investigated as a manufacturing method to produce LBM, since recent studies analyzing 3D bioprinting of bacteria, such as *Escherichia coli* (Lehner et al., 2017), *Bacillus subtilis* (Huang et al., 2019), or *Acetobacter xylinum* (Schaffner et al., 2017), demonstrated good cell viability and functionality over days up to several weeks. A blend of alginate and methylcellulose (algMC) was chosen as the hydrogel matrix of the LBM because it is a well-established bioink for extrusion-based bioprinting that exhibits high biocompatibility with various mammalian and non-mammalian cell types (Lode et al., 2015; Ahlfeld et al., 2017; Schütz et al., 2017; Dani et al., 2022). Alginate as a natural polymer has been used as an additive to mortar in several studies, which resulted in an increased compressive and tensile strength (Susilorini et al., 2014; Mohesson and Abbas, 2020) and enhances the building materials flame-, fire-, and heat-resistance significantly (DeBrouse, 2012). Further studies analyzed methylcellulose as an admixture to conventional concrete (Fu and Chung, 1998; Ahmed et al., 2021; Liu et al., 2021) and clay-based cementitious materials (Chen et al., 2020). It resulted in increased tensile strength, flexural properties, adhesion to steel reinforced concrete (Fu and Chung, 1998), enhanced plastic viscosity, and optimized rheological parameters for 3D printing applications of conventional concrete materials (Douba and Kawashima, 2021; Liu et al., 2021). Sea sand was added as a structural support component that should be consolidated by biomineralized CaCO_3 , as sand is a cheap commercial and common additive in construction materials such as concrete (Bos et al., 2016; Deutsches Institut für Normung, 2021). Rheological analyses revealed that up to 50 wt% sand can be added to the algMC ink, not affecting the shear-thinning behavior as an essential property for printability in extrusion-based 3D printing. At low shear rates (5 s^{-1}) the viscosity increased with increasing sand concentration. However, at high shear rates (100 s^{-1}) sand concentration did not affect the viscosity. These results are consistent with those of a study from Spangenberg et al. in which up to 50 wt% magnetite microparticles (mean diameter 25–30 μm) were incorporated into an algMC bioink while maintaining shear-thinning properties (Spangenberg et al., 2021). However, 3D printing of the bioinks with more than 25 wt% magnetite resulted in lower shape fidelity of the printed structures. In contrast, all hydrogels tested in this study exhibited good shear recovery properties and a high shape fidelity. Sand concentrations at and above 70 wt% resulted in stiff and brittle gels that were not printable. To make inks with higher solid particle concentrations printable, further adjustments would be required, such as varying the methylcellulose concentration and the particle size distribution. For further improvement of the environmental sustainability of the ink, alternative support materials to sea sand could be used, such as fly ash, cement kiln dust, silica fume, limestone, microfibers, or slag (Bos et al., 2016; Irfan et al., 2019; Kaufhold et al., 2019; Bhattacharjee et al., 2021; Booth and Jankovic, 2022).

Subsequently, algMC-based inks were tested with the cyanobacterium *Synechococcus* sp. strain PCC 7002 (further

referred to as PCC 7002). As the viability after the extrusion printing was still very high (86.8–92.6%) for all tested inks, PCC 7002 seem to tolerate the printing pressure during bioprinting. Even the addition of 50 wt% sand particles, which increase the shear forces during printing, did not reduce the viability of the cells. The significant increase in the chlorophyll content of the immobilized cells during the first 7 days of cultivation confirms the functionality of PCC 7002 regarding cell proliferation and photosynthetic activity. During prolonged cultivation, the cells increasingly grew out of the scaffolds with incorporated sand particles into the surrounding cell culture medium. This effect increased with higher sand concentrations. Since the methylcellulose is not crosslinked and remains soluble, it is washed out of the scaffolds into the medium with increasing cultivation time, leading to the formation of micropores (Ahlfeld et al., 2020), from which the cells can grow out of the scaffold. Since the sand particles also do not chemically react with the algMC matrix, this might lead to interstitial spaces and additional pores between the sand and the alginate network, increasing cell outgrowth. This effect could have led to the apparent decrease in viability after 14 days of cultivation between the bioink without and with 50 wt% of sand. To prevent the outgrowth, a thin dip coating with, for example, pure alginate could be used, which however might lead to a reduced exchange between the bioink strands and the surrounding medium. Additionally, cell viability of bioprinted PCC 7002 was also analyzed in mineralization medium, where it also was very high throughout the 14-day cultivation period (74.2–80.6%), confirming the stability of PCC 7002 against high salinities (Ludwig and Bryant, 2012). Since the mineralization process of cyanobacteria is fast and takes place within a few days or even hours, the viability tested in this study is considered high enough for the fabrication of the LBM (Heveran et al., 2020; Sidhu et al., 2022; Yang et al., 2022).

Through analysis of biomineralization in liquid culture, three different polymorphs were observed, namely, calcite, vaterite, and aragonite. It is known that different phases of CaCO_3 are formed during bacterial precipitation of calcium carbonate (Rodríguez-Navarro et al., 2007; Rodríguez-Navarro et al., 2012; Dhimi et al., 2013a; Hirsch et al., 2023), calcite and aragonite being the most abundant and stable ones (Leeuw and Parker, 1998). Interestingly, most of the natural occurrences of vaterite are associated with biogenic processes (Lippmann, 1973; Mann, 2005). Through scanning electron microscopy (SEM), structures surrounding the cells and interconnecting with the mineral phases were observed. The substances might be extracellular polymeric substances (EPS), which are known to be produced by a wide range of cyanobacteria (Nicolaus et al., 1999; Philippis et al., 2001; Pereira et al., 2009) and can largely influence the polymorphism of the precipitated CaCO_3 (Kawaguchi and Decho, 2002). Yu et al. reported the importance of the EPS produced by PCC 7002 for the sequestration of caesium ions due to several functional groups, such as amino-, hydroxyl-, and phosphate groups (Yu et al., 2020). Swanner et al. observed similar morphological structures and determined that they might be hydroxamate- and catechol-type siderophores, produced due to iron deficiency (Swanner et al., 2015). Machado et al. observed EPS-like fibrin structures in PCC 7002 cultures, as the bacteria were exposed to nano- and

micro-polyethylene particles (Machado et al., 2020). Chekroun et al. found that spherical vaterite is mainly present with live bacteria during mineralization (Chekroun et al., 2004). Vaterite production is strongly promoted by EPS (Naka and Chujo, 2001), especially by those presenting amino (Braissant et al., 2003; Ichikawa et al., 2003) or phosphate groups (Dupont et al., 1997; Sawada, 1997). These negatively charged groups could have attracted calcium ions and enhanced mineral formation in this study. However, further analysis must be done to identify and characterize the EPS-like structures.

Sidhu et al. analyzed the three-dimensional consolidation of a sand column through biomineralization by the cyanobacterium *Synechocystis pevalekii* and detected CaCO_3 precipitation plugging the pores between the sand particles. However, the consolidation was inhomogeneous because of the lack of light and aeration in parts of the column (Sidhu et al., 2022). 3D bioprinting could prevent these inhibitions through the incorporation of targeted macropores, i.e., the voids between the extruded strands. Therefore, after successful mineralization in liquid culture, the next step was to induce biomineralization in the bioprinted scaffolds to create the LBM. Mechanical testing, SEM imaging, and EDX measurements were performed to characterize the mineralization process and the resulting material composites. The uniaxial compression test of wet scaffolds showed that the maximum compressive strength of the LBM with PCC 7002 was higher than that of the abiotic control group without cells at each time point tested, namely, after 1, 7, and 14 days of cultivation in the mineralization medium. This increase indicates the promotion of mineralization by the incorporated bacteria. However, no further increase in compressive strength was measurable over time. This suggests that the mineralization process was already finished after 24 h, due to a potential equilibrium between calcium ions solidified in CaCO_3 and calcium ions crosslinking the alginate matrix, by forming egg-box junctions with the polyguluronate units of the alginate polysaccharide chains (Merakchi et al., 2019). To overcome this limitation, biomineralization could be designed as a multiple-step process in which new mineralization medium is added every 24 h, or as a continuous process in which the mineralization medium constantly flows through the porous scaffolds.

When testing the mechanical strength of air-dried samples, the abiotic control showed lower compressive strength with increasing sand concentration. This initially astonishing observation could be explained by the fact that the lower gel-to-sand ratio in the biomaterial blend with 50 wt% sand likely resulted in thinner (i.e., less stable) gel bridges between the sand particles, which break at lower stress than in the blend with 30 wt% sand. However, when PCC 7002 cells were added, the dependence reversed. This indicates that the bacteria-induced CaCO_3 mineralization was sufficient to consolidate the samples with a higher content of solid filler particles and therefore, a lower particle-to-particle distance that could be overcome by the biogenic mineral precipitates. Heveran et al. also confirmed the improvement of the mechanical strength of structures with PCC 7002, resulting in a 15% higher fracture energy for the LBM than for

the abiotic control (Heveran et al., 2020). Several other studies have revealed the importance of microorganisms in the mineralization process (Rodriguez-Navarro et al., 2007; Bundeleva et al., 2014). However, the microorganisms themselves may already be contributing to this effect (Skevi et al., 2021), as Zhang et al. observed a similar effect on fracture toughness when they compared the addition of a mineralizing strain and a wild-type control into a cementitious matrix (Zhang et al., 2019). Whether PCC 7002 actively or passively affected the mineralization processes and mechanical properties of the LBM in this study, is not yet clear. This could be further analyzed with a dead or inactivated cell control group.

SEM images showed that calcium carbonate precipitated in the LBM as well as in the abiotic control because the mineralization medium was supersaturated with calcium chloride and sodium bicarbonate. Since the outside scaffold serves as a nucleation point for the mineral production, a homogeneous mineral layer was observed across the entire surface. However, morphological differences between the biotic and abiotic samples inside the strands were evident in the scaffold cross-sections. The matrix between the sand particles in the abiotic control was smooth, and only few mineral particles were visible. In contrast, in the LBM CaCO_3 was found surrounding the cells and aligning along the alginate matrix between the sand grains, EDX measurements confirmed CaCO_3 precipitation. Obst et al. showed that CaCO_3 precipitates at the outer surface of the microorganism, interconnecting with the cyanobacterial EPS, possibly leading to changes in the mechanical properties of LBM compared to abiotic control samples (Obst et al., 2009).

In conclusion, the biomineralizing strain PCC 7002 was successfully incorporated into an alginate-based bioink containing up to 50 wt% sand as support material and macroporous scaffolds were fabricated by extrusion-based 3D bioprinting. The cells showed high viability in the immobilized state over a cultivation period of 14 days and remained functional regarding their MICP capability. Mineralized LBM were successfully fabricated and showed increased compressive strength when living cells were present. This indicates the consolidation of the sand particles through mineralized CaCO_3 , which presence was confirmed by microstructural analyses of the LBM.

Data availability statement

The raw data supporting the conclusion of this article will be made available by the authors, without undue reservation.

Author contributions

The manuscript was written by OR with contributions of all authors. All authors have given approval to the final version of the manuscript. Conceptualization and funding acquisition: MG, and MA; experimental work, data analysis, and visualization: OR; writing—original draft: OR; writing—reviewing and editing: MG, MA, SI, and OR; resources: MG.

Funding

This study has been funded by the German Federal Ministry for Education and Research (BMBF) in the frame of the BioCarboMin project (project No. 13XP5162A&B). The Article Processing Charges (APC) were funded by the joint publication funds of the TU Dresden, including Carl Gustav Carus Faculty of Medicine, and the SLUB Dresden as well as the Open Access Publication Funding of the DFG.

Acknowledgments

The authors want to thank the German Federal Ministry for Education and Research (BMBF) for financial support in the frame of the BioCarboMin project (project No. 13XP5162A&B). The project aims to develop novel biogenic building and construction materials using microbially induced calcium carbonate precipitation. After identifying suitable microorganisms, hydrogel-based immobilization media are mixed with specific filler materials and given into shape by 3D

References

- Ahlfeld, T., Cidonio, G., Kilian, D., Duin, S., Akkineni, A. R., Dawson, J. I., et al. (2017). Development of a clay based bioink for 3D cell printing for skeletal application. *Biofabrication* 9, 034103. doi:10.1088/1758-5090/aa7e96
- Ahlfeld, T., Guduric, V., Duin, S., Akkineni, A. R., Schütz, K., Kilian, D., et al. (2020). Methylcellulose - a versatile printing material that enables biofabrication of tissue equivalents with high shape fidelity. *Biomater. Sci.* 8, 2102–2110. doi:10.1039/d0bm00027b
- Ahlfeld, T., Köhler, T., Czichy, C., Lode, A., and Gelinsky, M. (2018). A methylcellulose hydrogel as support for 3D plotting of complex shaped calcium phosphate scaffolds. *Gels* 4, 68. doi:10.3390/gels4030068
- Ahmed, A., Ahmad, S., Mannal Kaleem, M., and Zahid, M. B. (2021). Experimental study on influence of methylcellulose on tensile and flexural strength of normal strength ordinary Portland cement concrete. *Mehran Univ. Res. J. Eng. Technol.* 40, 703–713. doi:10.22581/muet1982.2104.02
- Alsharif, A. F., Irwan, J. M., Othman, N., and Anneza, L. H. (2016). Isolation of sulphate reduction bacteria (SRB) to improve compress strength and water penetration of bio-concrete. *MATEC Web Conf.* 47, 01016. doi:10.1051/mateconf/20164701016
- Architecture (2022). Embodied carbon actions. Available at: <https://architecture2030.org/embodied-carbon-actions/> (Accessed September 26, 2022).
- Arp, G., Reimer, A., and Reitner, J. (2001). Photosynthesis-induced biofilm calcification and calcium concentrations in Phanerozoic oceans. *Science* 292, 1701–1704. doi:10.1126/science.1057204
- Badger, M. R., and Price, G. D. (2003). CO₂ concentrating mechanisms in cyanobacteria: Molecular components, their diversity and evolution. *J. Exp. Bot.* 54, 609–622. doi:10.1093/jxb/erg076
- Beatty, D. N., Williams, S. L., and Srubar, W. V. (2022). Biomineralized Materials for Sustainable and Durable Construction. *Annu. Rev. Mater. Res.* 52, 411–439. doi:10.1146/annurev-matsci-081720-105303
- Belie, N. de., Gruyaert, E., Al-Tabbaa, A., Antonaci, P., Baera, C., Bajare, D., et al. (2018). A Review of Self-Healing Concrete for Damage Management of Structures. *Adv. Mater. Interfaces* 5, 1800074. doi:10.1002/admi.201800074
- Bhattacharjee, S., Basavaraj, A. S., Rahul, A. V., Santhanam, M., Gettu, R., Panda, B., et al. (2021). Sustainable materials for 3D concrete printing. *Cem. Concr. Compos* 122, 104156. doi:10.1016/j.cemconcomp.2021.104156
- Booth, P., and Jankovic, L. (2022). Novel biodesign enhancements to at-risk traditional building materials. *Front. Built Environ.* 8, 766652. doi:10.3389/fbuil.2022.766652
- Bos, F., Wolfs, R., Ahmed, Z., and Salet, T. (2016). Additive manufacturing of concrete in construction: Potentials and challenges of 3D concrete printing. *Virtual Phys. Prototyp.* 11, 209–225. doi:10.1080/17452759.2016.1209867
- Braissant, O., Cailleau, G., Dupraz, C., and Verrecchia, E. P. (2003). Bacterially induced mineralization of calcium carbonate in terrestrial environments: The role of exopolysaccharides and amino acids. *J. Sediment. Res.* 73, 485–490. doi:10.1306/111302730485
- Bundeleva, I. A., Ménez, B., Augé, T., Bodéan, F., Recham, N., and Guyot, F. (2014). Effect of cyanobacteria *Synechococcus* PCC 7942 on carbonation kinetics of olivine at 20°C. *Miner. Eng.* 59, 2–11. doi:10.1016/j.mineng.2014.01.019
- Chekroun, K. B., Rodriguez-Navarro, C., Gonzalez-Munoz, M. T., Arias, J. M., Cultrone, G., and Rodriguez-Gallego, M. (2004). Precipitation and growth morphology of calcium carbonate induced by *myxococcus xanthus*: Implications for recognition of bacterial carbonates. *J. Sediment. Res.* 74, 868–876. doi:10.1306/050504740868
- Chen, Y., Chaves Figueiredo, S., Li, Z., Chang, Z., Jansen, K., Çopuroğlu, O., et al. (2020). Improving printability of limestone-calcined clay-based cementitious materials by using viscosity-modifying admixture. *Cem. Concr. Res.* 132, 106040. doi:10.1016/j.cemconres.2020.106040
- Concrete needs to lose its colossal carbon footprint (2021). Concrete needs to lose its colossal carbon footprint. *Nature* 597, 593–594. doi:10.1038/d41586-021-02612-5
- Dani, S., Windisch, J., Valencia Guerrero, X. M., Bernhardt, A., Gelinsky, M., Krujatz, F., et al. (2022). Selection of a suitable photosynthetically active microalgae strain for the co-cultivation with mammalian cells. *Front. Bioeng. Biotechnol.* 10, 994134. doi:10.3389/fbioe.2022.994134
- DeBrouse, D. R. (2012). *Alginate-based building materials: United States patent*. US008246733B2.
- DeJong, J. T., Mortensen, B. M., Martinez, B. C., and Nelson, D. C. (2010). Bio-mediated soil improvement. *Ecol. Eng.* 36, 197–210. doi:10.1016/j.ecoleng.2008.12.029
- Deutsches Institut für Normung (2021). *Beton: Festlegung, Eigenschaften, Herstellung und Konformität 91.100.30*. 206. Berlin: Beuth Verlag GmbH.
- Dhami, N. K., Reddy, M. S., and Mukherjee, A. (2013a). Biomineralization of calcium carbonate polymorphs by the bacterial strains isolated from calcareous sites. *J. Microbiol. Biotechnol.* 23, 707–714. doi:10.4014/jmb.1212.11087
- Dhami, N. K., Reddy, M. S., and Mukherjee, A. (2013b). Biomineralization of calcium carbonates and their engineered applications: A review. *Front. Microbiol.* 4, 314. doi:10.3389/fmicb.2013.00314
- Douba, A., and Kawashima, S. (2021). Use of nanoclays and methylcellulose to tailor rheology for three-dimensional concrete printing. *MJ* 118, 275–289. doi:10.14359/51733129
- Dupont, L., Portemer, F., and Figlarz, t. I. M. (1997). Synthesis and study of a well crystallized CaCO₃ vaterite showing a new habitus. *J. Mater. Chem.* 7, 797–800. doi:10.1039/a607761g
- Ersan, Y. C., Boon, N., and De Belie, N. (2015). “Microbial self-healing concrete: Denitrification as an enhanced and environment-friendly approach,” in 5th International Conference on Self-Healing Materials, Durham, USA, 22 – 24 June 2015.
- Falkowski, P. G. (1994). The role of phytoplankton photosynthesis in global biogeochemical cycles. *Photosynth Res.* 39, 235–258. doi:10.1007/BF00014586
- Foster, J. S., Green, S. J., Ahrendt, S. R., Golubic, S., Reid, R. P., Hetherington, K. L., et al. (2009). Molecular and morphological characterization of cyanobacterial diversity

bioprinting processes and conventional processes like casting, gelation, and freeze foaming. The fabrication step is followed by the MICP, leading to consolidated biogenic building and construction materials.

Conflict of interest

The authors declare that the research was conducted in the absence of any commercial or financial relationships that could be construed as a potential conflict of interest.

Publisher's note

All claims expressed in this article are solely those of the authors and do not necessarily represent those of their affiliated organizations, or those of the publisher, the editors and the reviewers. Any product that may be evaluated in this article, or claim that may be made by its manufacturer, is not guaranteed or endorsed by the publisher.

- in the stromatolites of Highborne Cay, Bahamas. *ISME J.* 3, 573–587. doi:10.1038/ismej.2008.129
- Fu, X., and Chung, D. D. L. (1998). Improving the bond strength of concrete to reinforcement by adding methylcellulose to concrete. *MJ* 95, 601–608. doi:10.14359/402
- Golubic, S. (1973). The relationship between blue-green algae and carbonate deposits. *Bot. Monogr.* 1973, 434–472.
- Guamán-Rivera, R., Martínez-Rocamora, A., García-Alvarado, R., Muñoz-Sanguinetti, C., González-Böhme, L. F., and Auat-Cheein, F. (2022). Recent developments and challenges of 3D-printed construction: A review of research fronts. *Buildings* 12, 229. doi:10.3390/buildings12020229
- Heveran, C. M., Williams, S. L., Qiu, J., Artier, J., Hubler, M. H., Cook, S. M., et al. (2020). Biomineralization and successive regeneration of engineered living building materials. *Matter* 2, 481–494. doi:10.1016/j.matt.2019.11.016
- Hirsch, M., Lucherini, L., Zhao, R., Clarà Saracho, A., and Amstad, E. (2023). 3D printing of living structural biocomposites. *Mater. Today* 62, 21–32. doi:10.1016/j.mattod.2023.02.001
- Huang, J., Liu, S., Zhang, C., Wang, X., Pu, J., Ba, F., et al. (2019). Programmable and printable *Bacillus subtilis* biofilms as engineered living materials. *Nat. Chem. Biol.* 15, 34–41. doi:10.1038/s41589-018-0169-2
- Chikawa, K., Shimomura, N., Yamada, M., and Ohkubo, N. (2003). Control of calcium carbonate polymorphism and morphology through biomimetic mineralization by means of nanotechnology. *Chemistry* 9, 3235–3241. doi:10.1002/chem.200204534
- IEA (2018). Technology roadmap - low-carbon transition in the cement industry. Available at: <https://www.iea.org/reports/technology-roadmap-low-carbon-transition-in-the-cement-industry> (Accessed September 26, 2022).
- Irfan, M. F., Hossain, S. M. Z., Khalid, H., Sadaf, F., Al-Thawadi, S., Alshater, A., et al. (2019). Optimization of bio-cement production from cement kiln dust using microalgae. *Biotechnol. Rep. (Amst)* 23, e00356. doi:10.1016/j.btre.2019.e00356
- Kamennaya, N., Ajo-Franklin, C., Northen, T., and Jansson, C. (2012). Cyanobacteria as Biocatalysts for Carbonate Mineralization. *Minerals* 2, 338–364. doi:10.3390/min2040338
- Kaufhold, J., Kohl, J., Nerella, V. N., Schroefl, C., Wenderdel, C., Blankenstein, P., et al. (2019). Wood-based support material for extrusion-based digital construction. *RPJ* 25, 690–698. doi:10.1108/RPJ-04-2018-0109
- Kawaguchi, T., and Decho, A. W. (2002). A laboratory investigation of cyanobacterial extracellular polymeric secretions (EPS) in influencing CaCO₃ polymorphism. *J. Cryst. Growth* 240, 230–235. doi:10.1016/S0022-0248(02)00918-1
- Kazemian, A., Yuan, X., Cochran, E., and Khoshnevis, B. (2017). Cementitious materials for construction-scale 3D printing: Laboratory testing of fresh printing mixture. *Constr. Build. Mater* 145, 639–647. doi:10.1016/j.conbuildmat.2017.04.015
- Kesti, M., Fisch, P., Pensalfini, M., Mazza, E., and Zenobi-Wong, M. (2016). Guidelines for standardization of bioprinting: A systematic study of process parameters and their effect on bioprinted structures. *BioNanoMaterials* 17. doi:10.1515/bnm-2016-0004
- Khalighi, S., and Saadatmand, M. (2021). Bioprinting a thick and cell-laden partially oxidized alginate-gelatin scaffold with embedded micro-channels as future soft tissue platform. *Int. J. Biol. Macromol.* 193, 2153–2164. doi:10.1016/j.ijbiomac.2021.11.046
- Khan, R., Jabbar, A., Ahmad, I., Khan, W., Khan, A. N., and Mirza, J. (2012). Reduction in environmental problems using rice-husk ash in concrete. *Constr. Build. Mater.* 30, 360–365. doi:10.1016/j.conbuildmat.2011.11.028
- Khoshnevis, B. (2004). Automated construction by contour crafting—Related robotics and information technologies. *Autom. Constr.* 13, 5–19. doi:10.1016/j.autcon.2003.08.012
- Kilian, D., Ahlfeld, T., Akkineni, A. R., Lode, A., and Gelinsky, M. (2017). Three-dimensional bioprinting of volumetric tissues and organs. *MRS Bull.* 42, 585–592. doi:10.1557/mrs.2017.164
- Labega-Martínez, N., Sanjurjo-Rivo, M., Díaz-Álvarez, J., and Martínez-Frías, J. (2017). Additive manufacturing for a Moon village. *Procedia Manuf.* 13, 794–801. doi:10.1016/j.promfg.2017.09.186
- Leeuw, N. H. de, and Parker, S. C. (1998). Surface structure and morphology of calcium carbonate polymorphs calcite, aragonite, and vaterite: An atomistic approach. *J. Phys. Chem. B* 102, 2914–2922. doi:10.1021/jp973210f
- Lehner, B. A. E., Schmieden, D. T., and Meyer, A. S. (2017). A straightforward approach for 3D bacterial printing. *ACS Synth. Biol.* 6, 1124–1130. doi:10.1021/acssynbio.6b00395
- Lippmann, F. (1973). *Sedimentary carbonate minerals*. Berlin, Heidelberg: Springer Berlin Heidelberg.
- Liu, C., Wang, X., Chen, Y., Zhang, C., Ma, L., Deng, Z., et al. (2021). Influence of hydroxypropyl methylcellulose and silica fume on stability, rheological properties, and printability of 3D printing foam concrete. *Cem. Concr. Compos.* 122, 104158. doi:10.1016/j.cemconcomp.2021.104158
- Lode, A., Krujatz, F., Brüggemeier, S., Quade, M., Schütz, K., Knaack, S., et al. (2015). Green bioprinting: Fabrication of photosynthetic algae-laden hydrogel scaffolds for biotechnological and medical applications. *Eng. Life Sci.* 15, 177–183. doi:10.1002/elsc.201400205
- Ludwig, M., and Bryant, D. A. (2012). *Synechococcus* sp. strain PCC 7002 transcriptome: Acclimation to temperature, salinity, oxidative stress, and mixotrophic growth conditions. *Front. Microbiol.* 3, 354. doi:10.3389/fmicb.2012.00354
- Krujatz, F., Dani, S., Windisch, J., Emmermacher, J., Hahn, F., Mosshammer, M., et al. (2022). Think outside the box: 3D bioprinting concepts for biotechnological applications - recent developments and future perspectives. *Biotechnology Advances* 58, 107930. doi:10.1016/j.biotechadv.2022.107930
- Machado, M. C., Vimbela, G. V., Silva-Oliveira, T. T., Bose, A., and Tripathi, A. (2020). The response of *Synechococcus* sp. PCC 7002 to micro-/nano polyethylene particles - investigation of a key anthropogenic stressor. *PLoS One* 15, e0232745. doi:10.1371/journal.pone.0232745
- Malda, J., Visser, J., Melchels, F. P., Jüngst, T., Hennink, W. E., Dhert, W. J. A., et al. (2013). 25th anniversary article: Engineering hydrogels for biofabrication. *Adv. Mater.* 25, 5011–5028. doi:10.1002/adma.201302042
- Mann, S. (2005). *Biomineralization: Principles and concepts in bioinorganic materials chemistry*. New York: Oxford University Press.
- Merakchi, A., Bettayeb, S., Drouiche, N., Adour, L., and Louncie, H. (2019). Cross-linking and modification of sodium alginate biopolymer for dye removal in aqueous solution. *Polym. Bull.* 76, 3535–3554. doi:10.1007/s00289-018-2557-x
- Merz, M. U. E. (1992). The biology of carbonate precipitation by cyanobacteria. *Facies* 26, 81–101. doi:10.1007/BF02539795
- Mitchell, A. C., and Ferris, F. G. (2005). The coprecipitation of Sr into calcite precipitates induced by bacterial ureolysis in artificial groundwater: Temperature and kinetic dependence. *Geochim. Cosmochim. Acta* 69, 4199–4210. doi:10.1016/j.gca.2005.03.014
- Mohesson, H. M., and Abbas, W. A. (2020). Effect of Biopolymer Alginate on some properties of concrete. *jcoeng* 26, 121–131. doi:10.31026/jcoeng.2020.06.10
- Murphy, S. V., and Atala, A. (2014). 3D bioprinting of tissues and organs. *Nat. Biotechnol.* 32, 773–785. doi:10.1038/nbt.2958
- Muynck, W. de., Belie, N. de., and Verstraete, W. (2010). Microbial carbonate precipitation in construction materials: A review. *Ecol. Eng.* 36, 118–136. doi:10.1016/j.ecoleng.2009.02.006
- Naka, K., and Chujo, Y. (2001). Control of crystal nucleation and growth of calcium carbonate by synthetic substrates. *Chem. Mater.* 13, 3245–3259. doi:10.1021/cr011035g
- Ngo, T. D., Kashani, A., Imbalzano, G., Nguyen, K. T., and Hui, D. (2018). Additive manufacturing (3D printing): A review of materials, methods, applications and challenges. *Compos. B. Eng.* 143, 172–196. doi:10.1016/j.compositesb.2018.02.012
- Nicolaus, B., Panico, A., Lama, L., Romano, I., Manca, M., Giulio, A., et al. (1999). Chemical composition and production of exopolysaccharides from representative members of heterocystous and non-heterocystous cyanobacteria. *Phytochemistry* 52, 639–647. doi:10.1016/S0031-9422(99)00202-2
- Noguchi, T., Kitagaki, R., and Tsujino, M. (2011). Minimizing environmental impact and maximizing performance in concrete recycling. *Struct. Concr.* 12, 36–46. doi:10.1002/suco.201100002
- Nomura, C. T., Sakamoto, T., and Bryant, D. A. (2006). Roles for heme-copper oxidases in extreme high-light and oxidative stress response in the cyanobacterium *Synechococcus* sp. PCC 7002. *Arch. Microbiol.* 185, 471–479. doi:10.1007/s00203-006-0107-7
- Nouri, H., Safedian, M., and Mir Mohammad Hosseini, S. M. (2021). Life cycle assessment of earthen materials for low-cost housing a comparison between rammed Earth and fired clay bricks. *Int. J. Build. Pathology Adapt.* ahead-of-print. doi:10.1108/IJBPA-02-2021-0021
- Obst, M., Wang, J., and Hitchcock, A. P. (2009). Soft X-ray spectro-tomography study of cyanobacterial biomineral nucleation. *Geobiology* 7, 577–591. doi:10.1111/j.1472-4669.2009.00221.x
- Panasar, D. K., and Zhang, R. (2020). Performance comparison of cement replacing materials in concrete: Limestone fillers and supplementary cementing materials – a review. *Constr. Build. Mater.* 251, 118866. doi:10.1016/j.conbuildmat.2020.118866
- Partensky, F., Hess, W. R., and Vaulot, D. (1999). *Prochlorococcus*, a marine photosynthetic prokaryote of global significance. *Microbiol. Mol. Biol. Rev.* 63, 106–127. doi:10.1128/MMBR.63.1.106-127.1999
- Paxton, N., Smolan, W., Böck, T., Melchels, F., Groll, J., and Jungst, T. (2017). Proposal to assess printability of bioinks for extrusion-based bioprinting and evaluation of rheological properties governing bioprintability. *Biofabrication* 9, 044107. doi:10.1088/1758-5090/aa8dd8
- Pentecost, A., and Riding, R. (1986). “Calcification in cyanobacteria,” in *Biomineralization in lower plants and animals* (United Kingdom: Systematics Association), 73–90.
- Pereira, S., Zille, A., Micheletti, E., Moradas-Ferreira, P., Philippis, R., and Tamagnini, P. (2009). Complexity of cyanobacterial exopolysaccharides: Composition, structures,

- inducing factors and putative genes involved in their biosynthesis and assembly. *FEMS Microbiol. Rev.* 33, 917–941. doi:10.1111/j.1574-6976.2009.00183.x
- Perito, B., and Mastromei, G. (2011). Molecular basis of bacterial calcium carbonate precipitation. *Prog. Mol. Subcell. Biol.* 52, 113–139. doi:10.1007/978-3-642-21230-7_5
- Philippis, R., Sili, C., Paperi, R., and Vincenzini, M. (2001). Exopolysaccharide-producing cyanobacteria and their possible exploitation: A review. *J. Appl. Phycol.* 13, 293–299. doi:10.1023/A:1017590425924
- Praveena, B., Lokesh, N., Abdulrajak, B., Santhosh, N., Praveena, B. L., and Vignesh, R. (2022). A comprehensive review of emerging additive manufacturing (3D printing technology): Methods, materials, applications, challenges, trends and future potential. *Mater. Today Proc.* 52, 1309–1313. doi:10.1016/j.matpr.2021.11.059
- Price, G. D., Badger, M. R., Woodger, F. J., and Long, B. M. (2008). Advances in understanding the cyanobacterial CO₂-concentrating-mechanism (CCM): Functional components, ci transporters, diversity, genetic regulation and prospects for engineering into plants. *J. Exp. Bot.* 59, 1441–1461. doi:10.1093/jxb/erm112
- Ribeiro, A., Blokzijl, M. M., Levato, R., Visser, C. W., Castilho, M., Hennink, W. E., et al. (2017). Assessing bioink shape fidelity to aid material development in 3D bioprinting. *Biofabrication* 10, 014102. doi:10.1088/1758-5090/aa90e2
- Robbins, L. L., and Blackwelder, P. L. (1992). Biochemical and ultrastructural evidence for the origin of whittings: A biologically induced calcium carbonate precipitation mechanism. *Geol* 20, 464. doi:10.1130/0091-7613(1992)020<0464:BAUEFT>2.3.CO;2
- Rodriguez-Navarro, C., Jimenez-Lopez, C., Rodriguez-Navarro, A., Gonzalez-Muñoz, M. T., and Rodriguez-Gallego, M. (2007). Bacterially mediated mineralization of vaterite. *Geochimica Cosmochimica Acta* 71, 1197–1213. doi:10.1016/j.gca.2006.11.031
- Rodriguez-Navarro, C., Jroundi, F., Schiro, M., Ruiz-Agudo, E., and Gonzalez-Muñoz, M. T. (2012). Influence of substrate mineralogy on bacterial mineralization of calcium carbonate: Implications for stone conservation. *Appl. Environ. Microbiol.* 78, 4017–4029. doi:10.1128/AEM.07044-11
- Rodriguez-Navarro, C., Rodriguez-Gallego, M., Ben Chekroun, K., and Gonzalez-Muñoz, M. T. (2003). Conservation of ornamental stone by *Myxococcus xanthus*-induced carbonate biomineralization. *Appl. Environ. Microbiol.* 69, 2182–2193. doi:10.1128/AEM.69.4.2182-2193.2003
- Sato, M., Murata, Y., Mizusawa, M., Iwahashi, H., and Oka, S. (2004). A simple and rapid dual-fluorescence viability assay for microalgae. *Microbiol. Cult. Collect.* 20, 53–59.
- Sawada, K. (1997). The mechanisms of crystallization and transformation of calcium carbonates. *Pure Appl. Chem.* 69, 921–928. doi:10.1351/pac199769050921
- Schaffner, M., Rühls, P. A., Coulter, F., Kilcher, S., and Studart, A. R. (2017). 3D printing of bacteria into functional complex materials. *Sci. Adv.* 3, ea06804. doi:10.1126/sciadv.aao6804
- Schindelin, J., Arganda-Carreras, I., Frise, E., Kaynig, V., Longair, M., Pietzsch, T., et al. (2012). Fiji: an open-source platform for biological-image analysis. *Nat Methods* 9, 676–682. doi:10.1038/nmeth.2019
- Schulze, K., López, D. A., Tillich, U. M., and Frohme, M. (2011). A simple viability analysis for unicellular cyanobacteria using a new autofluorescence assay, automated microscopy, and ImageJ. *BMC Biotechnol.* 11, 118. doi:10.1186/1472-6750-11-118
- Shutter, G., Lesage, K., Mechtcherine, V., Nerella, V. N., Habert, G., and Agusti-Juan, I. (2018). Vision of 3D printing with concrete — technical, economic and environmental potentials. *Cem. Concr. Res.* 112, 25–36. doi:10.1016/j.cemconres.2018.06.001
- Schütz, K., Placht, A.-M., Paul, B., Brüggemeier, S., Gelinsky, M., and Lode, A. (2017). Three-dimensional plotting of a cell-laden alginate/methylcellulose blend: Towards biofabrication of tissue engineering constructs with clinically relevant dimensions. *J. Tissue Eng. Regen. Med.* 11, 1574–1587. doi:10.1002/term.2058
- Seidel, J., Ahlfeld, T., Adolph, M., Kümritz, S., Steingroewer, J., Krutzat, F., et al. (2017). Green bioprinting: Extrusion-based fabrication of plant cell-laden biopolymer hydrogel scaffolds. *Biofabrication* 9, 045011. doi:10.1088/1758-5090/aa8854
- Sidhu, N., Goyal, S., and Reddy, M. S. (2022). Biomineralization of cyanobacteria *Synechocystis pevalekii* improves the durability properties of cement mortar. *Amb. Express* 12, 59. doi:10.1186/s13568-022-01403-z
- Skevi, L., Reeksting, B. J., Hoffmann, T. D., Gebhard, S., and Paine, K. (2021). Incorporation of bacteria in concrete: The case against MICP as a means for strength improvement. *Cem. Concr. Compos.* 120, 104056. doi:10.1016/j.cemconcomp.2021.104056
- Spangenberg, J., Kilian, D., Czichy, C., Ahlfeld, T., Lode, A., Günther, S., et al. (2021). Bioprinting of magnetically deformable scaffolds. *ACS Biomater. Sci. Eng.* 7, 648–662. doi:10.1021/acsbmaterials.0c01371
- Stevens, S. E., Patterson, C. O. P., and Myers, J. (1973). The production of hydrogen peroxide by blue-green algae: A survey. *J. Phycol.* 9, 427–430. doi:10.1111/j.1529-8817.1973.tb04116.x
- Strong, A. E., and Eadie, B. J. (1978). Satellite observations of calcium carbonate precipitations in the Great Lakes I. *Limnol. Oceanogr.* 23, 877–887. doi:10.4319/lo.1978.23.5.0877
- Susilorini, R. M. R., Hardjasaputra, H., Tudjono, S., Hapsari, G., Wahyu, S. R., Hadikusumo, G., et al. (2014). The advantage of natural polymer modified mortar with seaweed: Green construction material innovation for sustainable concrete. *Procedia Eng.* 95, 419–425. doi:10.1016/j.proeng.2014.12.201
- Swanner, E. D., Wu, W., Hao, L., Wüstner, M. L., Obst, M., Moran, D. M., et al. (2015). Physiology, Fe(II) oxidation, and Fe mineral formation by a marine planktonic cyanobacterium grown under ferruginous conditions. *Front. Earth Sci.* 3, 60. doi:10.3389/feart.2015.00060
- Tam, V. W. (2008). Economic comparison of concrete recycling: A case study approach. *Resour. Conservation Recycl.* 52, 821–828. doi:10.1016/j.resconrec.2007.12.001
- Tambunan, T., Juki, M. I., and Othman, N. (2019). Mechanical properties of sulphate reduction bacteria on the durability of concrete in chloride condition. *MATEC Web Conf.* 258, 01024. doi:10.1051/mateconf/201925801024
- Tetsch, L. (2016). Cyanobakterien: Symbiont mit globalem Einfluss. *Biol. Unserer Zeit* 46, 325–326. doi:10.1002/biuz.201690093
- Thompson, J. B., and Ferris, F. G. (1990). Cyanobacterial precipitation of gypsum, calcite, and magnesite from natural alkaline lake water. *Geol* 18, 995. doi:10.1130/0091-7613(1990)018<0995:CPOGCA>2.3.CO;2
- Thompson, J. B., Schultze-Lam, S., Beveridge, T. J., and Des Marais, D. J. (1997). Whiting events: Biogenic origin due to the photosynthetic activity of cyanobacterial picoplankton. *Limnol. Oceanogr.* 42, 133–141. doi:10.4319/lo.1997.42.1.0133
- Valot, L., Martinez, J., Mehdi, A., and Subra, G. (2019). Chemical insights into bioinks for 3D printing. *Chem. Soc. Rev.* 48, 4049–4086. doi:10.1039/C7CS00718C
- Wang, J. Y., Snoeck, D., van Vlierberghe, S., Verstraete, W., and Belie, N. de. (2014). Application of hydrogel encapsulated carbonate precipitating bacteria for approaching a realistic self-healing in concrete. *Construction and Building Materials* 68, 110–119. doi:10.1016/j.conbuildmat.2014.06.018
- Whitman, W. B., Coleman, D. C., and Wiebe, W. J. (1998). Prokaryotes: The unseen majority. *Proc. Natl. Acad. Sci. U. S. A.* 95, 6578–6583. doi:10.1073/pnas.95.12.6578
- Wu, P., Wang, J., and Wang, X. (2016). A critical review of the use of 3-D printing in the construction industry. *Autom. Constr.* 68, 21–31. doi:10.1016/j.autcon.2016.04.005
- Yang, G., Li, F., Deng, Z., Wang, Y., Su, Z., Huang, L., et al. (2022). Abnormal crystallization sequence of calcium carbonate in the presence of *Synechococcus* sp. PCC 7942. *Geomicrobiol. J.* 40, 34–45. doi:10.1080/01490451.2022.2100948
- Yu, R., Chai, H., Yu, Z., Wu, X., Liu, Y., Shen, L., et al. (2020). Behavior and mechanism of cesium biosorption from aqueous solution by living *Synechococcus* PCC7002. *Microorganisms* 8, 491. doi:10.3390/microorganisms8040491
- Zeybek, Ö., Özkılıç, Y. O., Karalar, M., Çelik, A. İ., Qaidi, S., Ahmad, J., et al. (2022). Influence of replacing cement with waste glass on mechanical properties of concrete. *Mater. (Basel)* 15, 7513. doi:10.3390/ma15217513
- Zhang, Z., Ding, Y., and Qian, S. (2019). Influence of bacterial incorporation on mechanical properties of engineered cementitious composites (ECC). *Constr. Build. Mater* 196, 195–203. doi:10.1016/j.conbuildmat.2018.11.089
- Zhu, T., and Dittrich, M. (2016). Carbonate precipitation through microbial activities in natural environment, and their potential in Biotechnology: A review. *Front. Bioeng. Biotechnol.* 4, 4. doi:10.3389/fbioe.2016.00004